



This open access document is posted as a preprint in the Beilstein Archives at <https://doi.org/10.3762/bxiv.2022.41.v1> and is considered to be an early communication for feedback before peer review. Before citing this document, please check if a final, peer-reviewed version has been published.

This document is not formatted, has not undergone copyediting or typesetting, and may contain errors, unsubstantiated scientific claims or preliminary data.

**Preprint Title** Enhanced electronic transport properties of Te roll-like nanostructures

**Authors** Emilson R. Viana, Nestor Cifuentes and Juan C. González

**Publication Date** 31 May 2022

**Article Type** Full Research Paper

**ORCID® iDs** Emilson R. Viana - <https://orcid.org/0000-0002-1883-3508>; Nestor Cifuentes - <https://orcid.org/0000-0003-3638-7959>

License and Terms: This document is copyright 2022 the Author(s); licensee Beilstein-Institut.

This is an open access work under the terms of the Creative Commons Attribution License (<https://creativecommons.org/licenses/by/4.0>). Please note that the reuse, redistribution and reproduction in particular requires that the author(s) and source are credited and that individual graphics may be subject to special legal provisions.

The license is subject to the Beilstein Archives terms and conditions: <https://www.beilstein-archives.org/xiv/terms>.

The definitive version of this work can be found at <https://doi.org/10.3762/bxiv.2022.41.v1>

## Enhanced electronic transport properties of Te roll-like nanostructures

*E. R. Viana*<sup>1\*</sup>, *N. Cifuentes*<sup>2</sup>, *J. C. González*<sup>2</sup>

<sup>1</sup> Departamento Acadêmico de Física, Universidade Tecnológica Federal do Paraná, Campus Curitiba, 80230-901, Curitiba, Brazil.

<sup>2</sup> Departamento de Física, Universidade Federal de Minas Gerais, 30123-970, Belo Horizonte, Brazil.

Keywords: *Tellurium, Nanobelts, Hopping Conduction, Electrical Characterization, Field Effect Transistors.*

\*Corresponding author: [emilsonjunior@professores.utfpr.edu.br](mailto:emilsonjunior@professores.utfpr.edu.br)

### Abstract

In this work, the electronic transport properties of Te roll-like nanostructures were investigated in a broad temperature range by fabricating single nanostructure back gated field-effect-transistors by photolithography. These one-dimensional nanostructures, with a unique roll-like morphology, were produced by a facile synthesis and extensively studied by scanning and transmission electron microscopy. The nanostructures are made of pure and crystalline Tellurium with trigonal structure (t-Te), and exhibit a p-type conductivity with enhanced field-effect hole mobility between 273 cm<sup>2</sup>/Vs at 320 K and 881 cm<sup>2</sup>/Vs at low 5 K. The thermal ionization of shallow acceptors, with a small ionization energy between 2 and 4 meV, leads to free hole conduction at high temperatures. The free hole mobility follows a negative power law temperature behavior, with exponent between -1.28 and -1.42, indicating strong phonon scattering in this temperature range. At lower temperatures, the electronic conduction is dominated by Nearest-Neighbor Hopping (NNH) conduction in the acceptors' band, with a small activation energy  $E_{\text{NNH}} \sim 0.6$  meV and acceptors concentration of  $N_{\text{A}} \sim 1 \times 10^{16}$  cm<sup>-3</sup>. These results demonstrate the enhanced electrical properties of these nanostructures, with a small disorder, and superior quality for nanodevice applications.

## 1. Introduction

The elemental chalcogen, Tellurium (Te), which is a rare element (0.002 ppm) in the Earth's crust and a well-known p-type and narrow band-gap (~0.35 eV at room temperature) semiconductor material. Tellurium is widely used in thermoelectric devices, piezoelectric devices, photoconductive devices, gas sensing, nonlinear optical devices, solar cells, photonic crystals, holographic recording devices, radioactive cooling devices, field-effect transistors, and infrared acoustic-optic deflectors [2-7].

Several chemical and physical methods have been recently developed to synthesize Te-based nanostructures, like monolayers (MLs), nanoparticles (NPs), nanorods (NRs), nanowires (NWs), nanobelts (NBs), nanotubes (NTs), nanoflowers (NF) and chiral nanostructures [6-10]. Trigonal-Tellurium (t-Te) MLs have also been recently proposed as a silicon successor for nanoelectronics because of their high hole mobility and current density [11]. Combining these electrical properties with the facile synthesis of one-dimensional nanostructure foresight potential applications of this material in nanoelectronic-optoelectronic integrated devices. However, a few works have been dedicated studying the electrical transport in Te-based one-dimensional nanostructures [12-15]. Te NTs have shown a metallic character and decreasing electrical resistivity with temperature [12]. Te NWs encapsulated in boron nitride nanotubes have shown a large current-carrying capacity and p-type semiconducting characteristics, that can be reversed to n-type behavior after Al<sub>2</sub>O<sub>3</sub> capping [13]. Theoretical works have also demonstrated that n-type single trigonal-Te NWs field-effect transistors (FETs) outperform the ones built on three trigonal Te NWs [15]. One important nanostructured group, different from hollow nanotubes and solid nanowires, corresponds to NBs. NBs have a well-defined geometry with a uniform rectangular cross-section along their entire length. This particular morphology establishes them as a strong candidate for providing a thorough understanding of dimensionally confined transport phenomena, as presented in SnO<sub>2</sub> NBs. Moreover, Strain-induced polarization charges have been studied in p-type Te NBs [14].

In this work, we have studied the electronic transport properties of a distinct one-dimensional t-Te nanostructure with a roll-like morphology, which resembles cinnamon sticks. The nanostructures were obtained by a facile PVP-assisted hydrothermal route

under mild conditions. A large quantity of these polycrystalline nanostructures with diameter between 100-900 nm and wall thickness around 50 nm were synthesized, and characterized by scanning electron microscopy (SEM), energy dispersive X-ray spectroscopy (EDS), transmission electron microscopy (TEM) and selected area electron diffraction (SAED). Individual Te roll-like nanobelts were connected in back-gate FETs and measured to characterize the electronic transport as a function of temperature. To our best knowledge, the electronic transport in Te roll-like one-dimensional nanowires have not been achieved so far.

## **2. Methodology**

### **2.1. Growth of Te roll-like one-dimensional nanostructures.**

Te nanostructures were grown by an environmentally friendly solvothermal method by the reduction of  $\text{Na}_2\text{TeO}_3$  and passivation with Polyvinylpyrrolidone (PVP), reported elsewhere [16]. The procedure described Wu et al. [16] for the synthesis Te NWs was followed, with the modification of increasing the autoclave heating to 200 °C. All reagents used were analytic grade, purchased from Sigma-Aldrich Chemicals Company<sup>®</sup>, and directly used without further purification.

### **2.2 Morphology, elemental analysis, and crystal structure.**

The morphology and elemental analysis of the as-prepared products were characterized by scanning electron microscopy (SEM, FEI Quanta 3D FEG) at an acceleration voltage of 15.0 kV. An EDS system attached to the SEM was employed to analyze the chemical composition. Transmission electron microscopy (TEM), high-resolution transmission electron microscopy (HRTEM) images, and selected area electron diffraction (SAED) measurements were carried out in a FEI Tecnai G2-20 S-TWIN operated at 200 kV in a bright-field (BF) TEM mode. EDS point acquisitions were also performed during TEM analysis by using a silicon drift detector (SDD) from Oxford Instruments.

### **2.3. Electronic transport.**

The electronic transport properties of the sample were investigated by acquiring and modeling the transfer and gate curves of Te roll like single nanostructure back gate FETs, as well as the electrical resistivity of the nanostructures as a function of temperature from 5K to 400 K. The transport measurements were carried out in a low-noise homemade system for electrical characterization of FETs devices [17-19]. FETs devices were built

by laser writing optical lithography on  $1 \times 1 \text{ cm}^2$  degenerate Si (100) substrates covered by a 300 nm thick high-quality  $\text{SiO}_2$  layer. A Cr(10 nm)/Au(100 nm) bilayer was thermally evaporated on the sample to produce good Ohmic contacts. This procedure follows the methodology developed for single nanobelt back gated FETs [17-20].

### 3. Results and Discussion

The morphology of the as-prepared Te roll-like one-dimensional nanostructures is shown in Figure 1. Figures 1(a) and 1(b) display a representative overview of the nanostructures, which shows that the prepared samples are composed of large-scale roll-like one-dimensional nanostructures. Most nanostructures exhibit a flat end and a tip at the other extreme. The size distribution of the nanostructures is shown in the inset of Figure 1(b), with a mean diameter of around 550 nm. Due to the tip at the end of the nanostructures, the diameters were measured at approximately the center part, where the size is uniform. The wall thickness of the nanostructures was found between 45 nm and 55 nm.

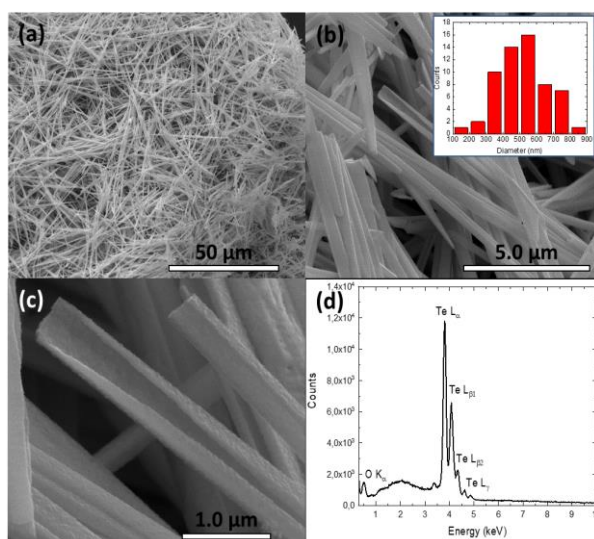


**Figure 1.** SEM images at different magnifications of the roll-like Te nanostructures (a)-(c) and (d) the EDS spectra of the sample. In the inset of (b), the histogram of the diameter distribution of the nanostructures.

Figure 1(c) shows a high-magnification SEM image of the nanostructures, which vividly demonstrates the surface rugosity and the lateral opening along the growth axis of the roll-like structure. Elemental analysis of the nanostructures is shown in Figure 1(d), where the strong Te peaks and a residual oxygen peak in the EDS spectrum demonstrate the chemical composition of the nanostructures. To our best knowledge, this morphology has not been reported for hydrothermal synthesis of Te nanostructures. Though, similar

morphologies have been observed in Te scroll-like nanostructures grown by reflux processes [21] or Te shuttle-like scrolled nanostructures produced by amino acids controlled hydrothermal growth [22]. However, the typical seed at the center of the scroll-like nanostructure grown by reflux processes was not observed in our case, nor characteristic sharp tip at both ends of the shuttle-like scrolled Te NTs.

Figure 2 shows TEM images and the corresponding SAED patterns of the roll-like Te nanostructure. The SAED patterns shown in Figure 2(b)/2(d) were acquired from the marked circular area in Figure 2(a)/2(c), respectively. Next to the tip of the nanostructure, in Figure 2(b), and next to the flat end of the nanostructure in Figure 2(d). Detailed analysis of the SAED patterns, acquired along the  $[-1-20]$  zone axis, using CrysTBox software [23, 24] demonstrate that the roll-like nanostructure is crystalline. The one-dimensional nanostructure was found to present the trigonal crystal structure of bulk Te, growing in the  $[001]$  orientation (indicated by a white arrow in the SAED patterns) along the longitudinal direction (parallel to the axis of the Te nanostructure) and  $[210]$  growth toward the transverse direction (perpendicular to the growth axis). The  $[001]$  growth direction is usually observed in one-dimensional t-Te nanostructures and attributed to the anisotropy of Te crystal structure [21, 22]. However, a Fast Fourier transform (FFT) analysis of different areas of HRTEM images (see Figure 3(a)) shows that the nanostructures are polycrystalline, with well-oriented large grains and rotated small grains at the edges. Small amorphous areas were observed at the edges of the nanostructures. However, the well-defined SAED spot patterns of Figure 2(b) and 2(d), as well the FFT patterns in Figure 3(a) are a clear indication of the crystalline nature of the nanostructures. The expected diffuse halo or broad circles associated with the diffraction of amorphous/nanocrystalline materials [25] were not observed. The EDS point analysis (see Figure 3(b)) shows that nanostructures are constituted by Te, in agreement with the results of the SAED analysis and the above presented EDS analysis of the sample, fig.1(d).

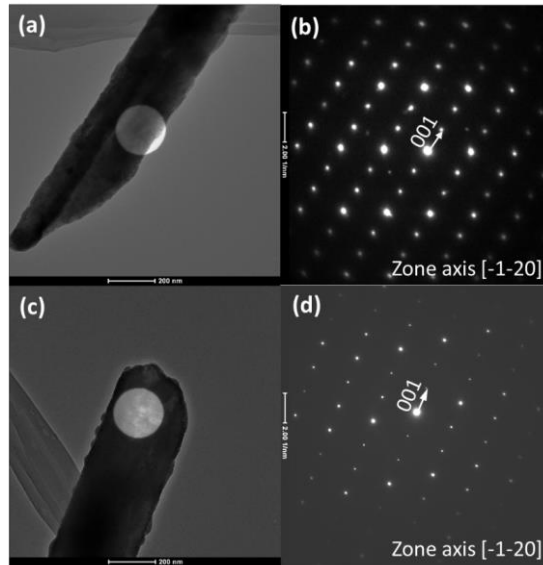


**Figure 2.** TEM image and SAED patterns of the flat end, (a) and (b), and tip, (c) and (d), of a roll-like t-Te one-dimensional nanostructure.

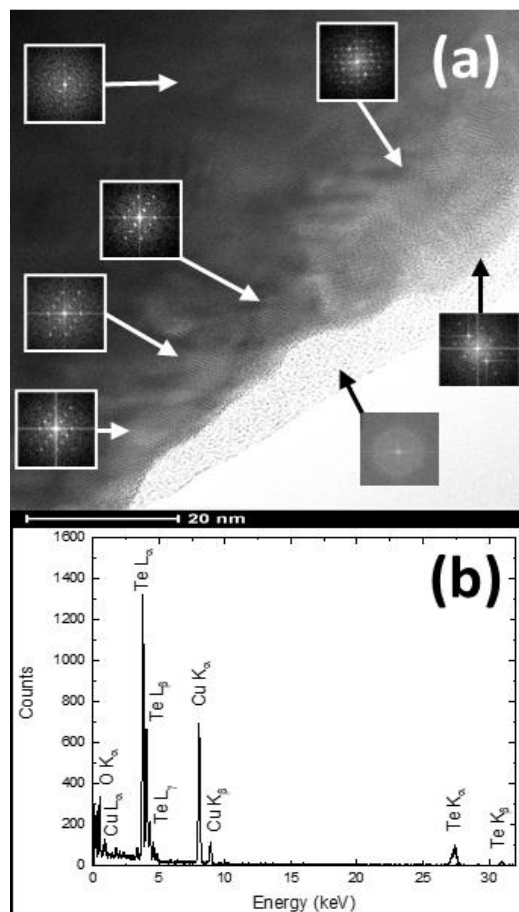


**Figure 3.** (a) HRTEM image of the roll-like t-Te one-dimensional nanostructure with FFT patterns in different regions of the sample. (b) The EDS spectra of the corresponding nanostructure.

The transfer characteristics of the t-Te NW-1 roll like FET ( $I_{ds} - V_g$  curve) at 320 K and 5 K are shown in Figure 4 for  $V_{ds} = 10$  mV. There is a strong increase of the transconductance ( $g_m = d(I_{ds})/d(V_g)$ ) of approximately 30x, from 0.53 nA/V at 300 K to 17 nA/V at 5 K. The p-type character of the NW is clear from these curves. Recently, band structure calculations of t-Te have revealed that a unique structure of the valence band at the H point in the Brillouin zone provides conduction channels for holes [26, 27]. The fourfold degenerate valence band, at the H point, is split into two non-degenerate H4 and H5 bands and a doubly degenerate lower H6 band, due to the strong spin-orbit coupling in the Te. Both the H4 and H5 bands lie close to the Fermi level and therefore contribute to hole transport, while the H6 band lies at a lower energy position and does not significantly contribute holes to the conduction.

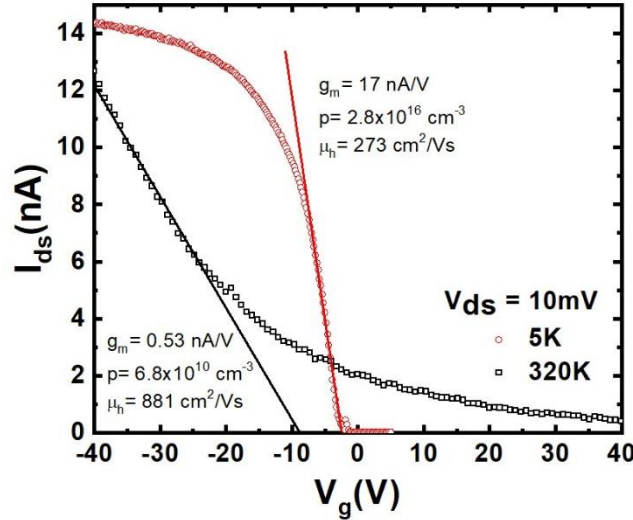


**Figure 4.** The transfer characteristic ( $I_{ds}-V_g$ ) of a single roll-like t-Te NW-1 one-dimensional nanostructure back gated FET acquired at 5K and 320 K.

Field effect hole mobility ( $\mu_h$ ) and concentration ( $p$ ) were estimated from the  $I_{ds}-V_g$  curve using a parallel capacitor model for the FET [20, 28]. This model has been successfully used to analyze the electronic properties of single semiconductor NWs of different cross-sections and materials such as ZnO [28], SnO<sub>2</sub> [17, 20] and GaAs [18, 19, 29]. In this case, the calculations were done using  $\mu_h = g_m L^2 / (V_{ds} C_{ox})$  and  $p = 1 / (e \rho \mu_h)$ ,

where  $g_m = dI_{ds}/dV_g$  is the transconductance,  $\rho$  is the resistivity,  $C_{ox}$  is the gate capacitance, and  $e$  is the electronic charge. For a flat nanostructure, the gate capacitance can be obtained by a simple parallel plate approximation, given by  $C_{ox} = \epsilon_0(\epsilon_{av})wL/d_{SiO_2}$ , and  $\rho = (R.w.t/L)$ . Where  $\epsilon_0$  is the permittivity of free space,  $\epsilon_{av} = 1.95$  is the averaged relative permittivity of  $SiO_2$  /air interface for the FET [20, 30],  $w = 550$  nm,  $t = 50$  nm, and  $L = 5.97$   $\mu$ m, are the diameter and thickness of the nanostructure, and the length of the FET channel, respectively. The thickness of the dielectric layer ( $SiO_2$ ) in the capacitor is  $d_{SiO_2} = 300$  nm.

Figure 4 shows the transfer curves ( $I_{ds}$ - $V_g$ ) of a single roll-like t-Te NW-1 one-dimensional nanostructure back gated FET acquired at 5K and 320 K, as well as the calculated values of  $g_m$ ,  $p$  and  $\mu_h$ . The hole mobility was estimated to be  $\mu_h(320$  K) = 273  $cm^2/Vs$  and  $\mu_h(5$  K) = 881  $cm^2/Vs$ , while the hole concentration was estimated to be  $p(320$  K) =  $2.8 \times 10^{16}$   $cm^{-2}$  and  $p(5$  K) =  $6.8 \times 10^{10}$   $cm^{-3}$ .

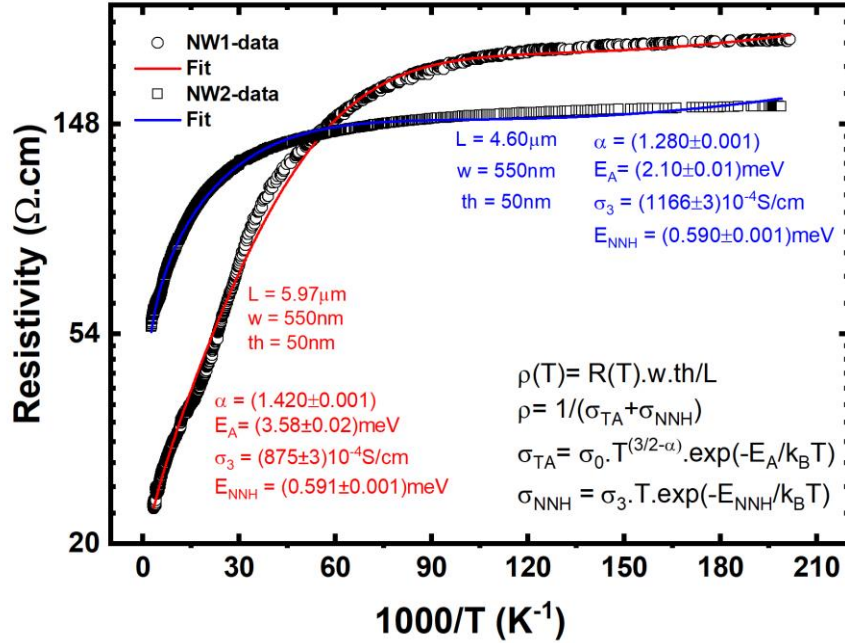


**Figure 5.** Resistivity as a function of temperature for the t-Te roll-like NW-1 and NW-2.

The measured electrical resistivity of NW-1 and NW-2, as a function of temperature, from 300K down to 5K, is shown in Figure 5. Two linear regions can be observed at high and low temperatures, corresponding to the thermally activated conduction ( $\sigma_{TA}$ ) of free holes and the nearest-neighbor hopping (NNH,  $\sigma_{NNH}$ ) [31-34], respectively.

In the high-temperature region, the thermally activated conduction can be expressed as [34]:

$$\sigma_{TA}(T) = e\mu_h(T)p(T) \quad (\text{eq.1})$$

$$\mu_h(T) \approx \mu_0 T^{-\alpha} \quad (\text{eq.2})$$

$$p(T) \approx N_V^{eff} T^{3/2} e^{-\frac{E_A}{k_B T}} \quad (\text{eq.3})$$

where  $\mu_0$  is a constant. Since the mobility is mainly limited by phonon scattering at high temperatures,  $\alpha$  is close to 3/2 [34, 35].  $N_V^{eff}$  is the effective density of states of the valence band,  $E_A$  is the shallow acceptor ionization energy [34], and  $k_B$  is the Boltzmann's constant.

At lower temperatures, most of the free holes are recaptured by the acceptors and cannot be thermally excited back to the valence band [31, 34]. In this case, the thermally activated conduction of free holes becomes less important, and hole hopping directly between acceptor states in the impurity band becomes the primary conduction mechanism [31-34].

In this case, conduction is realized through NNH of charge carriers with small activation energy directly over impurity states. The conductivity in the NNH model is given by [36]:

$$\sigma_{NNH}(T) = \sigma_3 T e^{-\frac{E_{NNH}}{k_B T}} \quad (\text{eq.4})$$

$$E_{NNH} = \frac{0.99e^2 N_A^{1/3}}{4\pi\epsilon_0\epsilon_r} \quad (\text{eq.5})$$

where  $\sigma_3$  is a constant,  $E_{NNH}$  is the activation energy for NNH conduction,  $N_A$  is the acceptor concentration, and  $\epsilon_r = 53.5$  is the relative permittivity of t-Te [37].

Considering both TA and NNH conduction mechanisms, it is possible to extract some of the above-mentioned parameters by fitting the resistivity data of NW-1 and NW-2 (fig.5) with  $\rho(T) = [1/[\sigma_{TA}(T) + \sigma_{NNH}(T)]]$ . This model explains well our NW-1 and NW-2 data over the whole temperature range. To our best knowledge, the ionization energy of shallow acceptors has not been reported for t-Te nanostructures. The ionization energy of shallow acceptors can be calculated, as being 4 meV, from the hydrogenic model [34] using the holes effective mass  $m_h = 0.91m_0$  for t-Te [38]. The theoretical value is in excellent agreement with our experimental values of  $E_A = 2.10$  meV and  $E_A = 3.58$ meV,

found through the analysis of the resistivity data (Fig.5). These values are surprisingly small compared to the larger ionization energy of acceptors (near 1 eV) in semiconductors with small valence band effective mass [39, 40]. However, the very large relative permittivity of t-Te,  $\epsilon_r = 53.5$ , should also be considered.

The temperature dependence of the hole mobility in t-Te one-dimensional nanostructures has not been reported to the best of our knowledge. However, for bulk crystals and temperatures above 77 K, a power-law  $\mu \sim T^{-1.5}$  [38] or weaker was registered in the literature [35, 41]. The power-law strongly depends on the doping level of the t-Te crystals [35]. In our case, a weaker dependency with  $\alpha = (1.420 \pm 0.001)$  and  $(1.280 \pm 0.001)$ , (Eq.2), for NW-1 and NW-2, was found, demonstrating strong scattering by phonons in this temperature range.

At lower temperatures, the electronic conduction is dominated by NNH in the acceptors band with a low activation energy  $E_{NNH} \sim 0.59$  meV for both NWs. These values of  $E_{NNH}$  correspond to a concentration of acceptors of  $N_A \sim 1 \times 10^{16}$  cm<sup>-3</sup> for both NWs. Due to the small acceptor ionization energy, the acceptor band will be completely ionized at high temperatures, and the acceptor concentration can be compared with the hole concentration found at 320 K ( $2.8 \times 10^{16}$  cm<sup>-2</sup>). These values are in excellent agreement, corroborating our interpretation of the temperature dependence of resistivity.

The temperature behavior of the resistivity of the t-Te roll-like nanostructures is somehow different than previously reported for t-Te bulk crystals and NWs. The first striking characteristic of previous reports is the metallic-like character of some bulk crystals [35, 41, 42] and NWs [45] at high temperatures, revealed by a decrease the electrical resistance as the temperature drops. This behavior is not observed in our material, which presents a semiconductor behavior over the whole investigated temperature range. At low temperatures, the electronic conduction in t-Te bulk [46, 47] and NWs [45] has been associated with variable range hopping (VRH). VRH conduction of Mott ( $\sigma_M \sim \exp(T_M/T)^{1/4}$ ) and Efros-Shklovskii ( $\sigma_{ES} \sim \exp(T_{ES}/T)^{1/2}$ ) types has also been reported in chalcogenide semiconducting materials [30, 32] and one-dimensional nanostructures [18, 19, 29, 48]. However, VRH was not observed in our t-Te roll like NWs, indicating low disorder in these nanostructures. Mobility values of more than 700 cm<sup>2</sup>/Vs have also been reported at room temperature for t-Te NWs [59]. However, in this case, the mobility was determined for elevated values of  $V_g$ , apparently far from the linear

region of the FET transfer characteristic. Other authors have reported t-Te NWs hole mobilities between  $72 \text{ cm}^2/\text{Vs}$  and  $349 \text{ cm}^2/\text{Vs}$ , for carrier concentration in the range of  $10^{18} \text{ cm}^{-3}$  using the transconductance obtained from the linear region of the transfer characteristic of the FETs [51-52]. Our reported values are significantly higher at 320 K ( $273 \text{ cm}^2/\text{Vs}$ ) and particularly at 5 K ( $881 \text{ cm}^2/\text{Vs}$ ), but for lower carrier concentrations,  $\sim 1 \times 10^{16} \text{ cm}^{-3}$ .

#### **4. Conclusions**

In summary, we have demonstrated the facile synthesis of morphologically unique roll-like nanostructures. Extensive electron microscopy studies confirm that these nanostructures are made of pure and crystalline Te with trigonal structure. The electronic transport properties of these nanostructures were investigated in a broad temperature range by fabricating single nanobelt back gated FET devices on  $\text{SiO}_2/\text{Si}$  substrates. These nanostructures exhibit a p-type conductivity with superior room temperature field-effect hole mobility compared to bulk and nanostructures of Te previously synthesized by other methods. The analysis of the temperature dependence of the electrical resistivity shows that at high temperature, the conduction is done by free holes ionized from shallow acceptors with ionization energy between  $E_A = 2.10$  to  $3.58 \text{ meV}$ , in agreement with the expected value from the hydrogenic model. Elevated free hole mobility was also found ( $\mu_h(320 \text{ K}) = 273 \text{ cm}^2/\text{V.s}$ ,  $\mu_h(5 \text{ K}) = 881 \text{ cm}^2/\text{V.s}$ ) in these nanostructures. These superior quality transport properties demonstrate the potential use of t-Te roll-like nanostructure for electronic device applications.

#### **Acknowledgments**

This work was supported by the Conselho Nacional de Desenvolvimento Científico e Tecnológico (CNPq) under grant nos. 406139/2018-0, 305808/2018-4. The authors acknowledge the financial support of CAPES, Fundação de Amparo à Pesquisa do Estado de Minas Gerais (FAPEMIG) under the grant APQ-03044-17, and Fundação Araucária. The authors thank Prof. Geraldo Mathias Ribeiro for the synthesis of the nanostructures. The authors also thank Prof. Daniel Bretas Roas and the Center of Microscopy at the Universidade Federal de Minas Gerais (CM-UFMG) for the electron microscopy measurements and TEM sample preparation.

## References

- [1] B. Zare, Z. Sepehrizadeh, M. A. Faramarzi, M. SoltanyRezaee-Rad, S. Rezaie and A. R. Shahverdi, *Biotechnol. Appl. Biochem.* **2014**, *61*, 395–400. <https://doi.org/10.1002/bab.1180>
- [2] H. Muhammad, H. Zhen, C. Jia-Fu, L. Jian-Wei, Y. Shu-Hong, *Tellurium Nanostructures: Synthesis, Properties, and their applications*. Doris Grey. Nova Science Publisher, New York, USA, ISBN:978-1-53610-555-1, **2017**.
- [3] Kramer, A., Van de Put, M.L., Hinkle, C.L. et al.. *npj 2D Mater Appl* **2020**, *4*, 10 (2020). <https://doi.org/10.1038/s41699-020-0143-1>.
- [4] O. de Melo, M. Behar, J. Ferraz Dias, R. Ribeiro-Andrade, M.I.N. da Silva, A.G. de Oliveira, J.C. González. *Materials Science in Semiconductor Processing* **2019**, *97*, 17-20. <https://doi.org/10.1016/j.mssp.2019.02.034>.
- [5] O. de Melo, A. Domínguez, K. Gutiérrez Z-B, G. Contreras-Puente, S. Gallardo-Hernández, A. Escobosa, J. C. González, R. Paniago, J. Ferraz Dias, M. Behar. *Solar Energy Materials and Solar Cells* **2015**, *138*, 17-21. <https://doi.org/10.1016/j.solmat.2015.02.025>.
- [6] O. de Melo, L. García-Pelayo, Y. González, O. Concepción, M. Manso-Silván, R. López-Nebreda, J. L. Pau, J. C. González, A. Climent-Fontae, V. Torres-Costa. *J. Mater. Chem. C* **2018**, *6*, 6799-6807. <https://doi.org/10.1039/C8TC01685B>.
- [7] E. Sánchez-Montejo, G. Santana, A. Domínguez, L. Huerta, L. Hamui, M. López-López, H. Limborço, F. M. Matinaga, M.I.N. da Silva, A. G. de Oliveira, J. C. González, O. de Melo. *Materials Chemistry and Physics* **2017**, *198*, 317-323. <https://doi.org/10.1016/j.matchemphys.2017.06.031>.
- [8] E. Piacenza, A. Presentato, E. Zonaro, S. Lampis, G. Vallini, R. J. Turner. *Phys. Sci. Rev.* **2018**, *3*, 20170100. <https://doi.org/10.1515/psr-2017-0100>.
- [9] J-W. Liu, J. Xu, W. Hu, J.-L. Yang, S.-H. Yu. *Chem Nano Mat.* **2016**, *2*, 167 – 170. <https://doi.org/10.1002/cnma.201500206>.
- [10] Z. He, Y. Yang, J.-W. Liu, S.-H. Yu. *Chem. Soc. Rev.* **2017**, *46*, 2732. <https://doi.org/10.1039/c7cs00013h>.
- [11] Kramer, A., Van de Put, M.L., Hinkle, C.L. et al. *npj 2D Mater Appl* **2020**, *4*, 10. <https://doi.org/10.1038/s41699-020-0143-1>
- [12] W. H. Xu, J. M. Song, L. Sun, J. L. Yang, W. P. Hu, Z. Y. Ji and S. H. Yu, *Small*, **2008**, *4*, 888–893. <https://doi.org/10.1002/sml.200701227>
- [13] Qin, JK., Liao, PY., Si, M. et al. *Nature Electronics* **2020**, *3*, 141–147. <https://doi.org/10.1038/s41928-020-0365-4>
- [14] S. Gao, Y. Wang, R. Wang, W. Wu. *Semicond. Sci. Technol.* **2017**, *32*, 104004. <https://doi.org/10.1088/1361-6641/aa8605>
- [15] Y. Yin, Z. Zhang, H. Zhong, C. Shao, X. Wan, C. Zhang, J. Robertson, Y. Guo. *ACS Appl. Mater. Interfaces* **2021**, *13*, 3387–3396. <https://doi.org/10.1021/acsami.0c18767>

- [16] Wu, X., Yuan, L., Zhou, S. et al. *J. Nanopart. Res.* **2012**, *14*, 1009. <https://doi.org/10.1007/s11051-012-1009-z>
- [17] E. R. Viana, J. C. González, G. M. Ribeiro, A. G. de Oliveira. *Nanoscale* **2013**, *5*, 6439-6444. <https://doi.org/10.1039/C3NR01300F>
- [18] N. Cifuentes, H. Limborco, E. R. Viana, D. Roa, A. Abelenda, M. da Silva, M. Moreira, G. M. Ribeiro, A. G. de Oliveira, J. C. González. *J. Phys. Status Solidi B* **2016** *10*, 1960–1964. <https://doi.org/10.1002/pssb.201600204>
- [19] N. Cifuentes, E. R. Viana, H. Limborco, D. B. Roa, A. Abelenda, M. da Silva, M. Moreira, G. M. Ribeiro, A. G. de Oliveira, J. C. González. *J. Nanomater.* **2016**, 9451319. <https://doi.org/10.1155/2016/9451319>
- [20] E. R. Viana, G. M. Ribeiro, A. G. de Oliveira, J. C. González. *Nanotechnology* **2017**, *28*, 445703. <https://doi.org/10.1088/1361-6528/aa871a>
- [21] W. Zhu, W. Wang, H. Xu, L. Zhou, L. Zhang, J. Shi. *Crystal Growth & Design* **2006**, *6*, 2804. <https://doi.org/10.1021/cg060439o>
- [22] Z. He, S.-H. Yu, J. Zhu. *Chem. Mater.* **2005**, *17*, 2785. <https://doi.org/10.1021/cm0503228>
- [23] M. Klinger. *J. of Appl. Cryst.* **2017**, *50*, 1226-1234. <https://doi.org/10.1107/S1600576717006793>
- [24] M. Klinger and A. Jäger. *J. Appl. Cryst.* **2015**, *48*(6), 2012-2018. <https://doi.org/10.1107/S1600576715017252>.
- [25] J. C. González, H. Limborço, R. Ribeiro-Andrade, B. C. Silva, K. Krambrock. *Adv. Electron. Mater.* **2022**, *8*, 2100985. <https://doi.org/10.1002/aelm.202100985>.
- [26] H. Peng, N. Kioussis, and G. J. Snyder, *Phys. Rev. B* **2014**, *89*(19), 195206.
- [27] L. A. Agapito, N. Kioussis, W. A. Goddard III, N. P. Ong. *Phys. Rev. Lett.* **2013**, *110*(17), 176401. <https://doi.org/10.1103/PhysRevLett.110.176401>
- [28] K. R. Sapkota, W. Chen, F. S. Maloney, U. Poudyal, and W. Wang, *Sci. Rep.* **2016**, *6*, 35036. <https://doi.org/10.1038/srep35036>
- [29] P. Kannappan, N. B. Sedrine, J. P. Teixeira<sup>1</sup>, M. R. Soares, B. P. Falcão, M. R. Correia, N. Cifuentes, E. R. Viana, M. V. B. Moreira, G. M. Ribeiro, A. G. de Oliveira, J. C. González, J. P. Leitão. *Beilstein J. Nanotechnol.* **2017**, *8*, 2126. <https://doi.org/10.3762/bjnano.8.212>
- [30] Daryoosh Vashaee, Ali Shakouria, Joshua Goldberger, Tevye Kuykendall, Peter Pauzauskie, and Peidong Yang. *J. Appl. Phys.* **2006**, *99*, 054310. <https://doi.org/10.1063/1.2168229>
- [31] N. Cifuentes, S. Ghosh, A. Shongolova, M. R. Correia, P. M. P. Salomé, P. A. Fernandes, S. Ranjbar, S. Garud, B. Vermang, G. M. Ribeiro, J. C. González. *J. Phys. Chem. C* **2020**, *124*, 7677. <https://doi.org/10.1021/acs.jpcc.0c00398>
- [32] J. C. González, G. M. Ribeiro, E. R. Viana, P. A. Fernandes, P. M. P. Salomé, K. Gutiérrez, A. Abelenda, F. M. Matinaga, J. P. Leitão, A. F. da Cunha. *J. Phys. D: Appl. Phys.* **2013**, *46*, 155107. <https://doi.org/10.1088/0022-3727/46/15/155107>

- [33] A. Shongalova, M. R. Correia, J. P. Teixeira, J. P. Leitão, J. C. González, S. Ranjbar, S. Garud, Vermang, J. M. V. Cunha, P. M. P. Salomé, P. A. Fernandes. *Solar Energy Materials and Solar Cells* **2018**, *187*, 219. <https://doi.org/10.1016/j.solmat.2018.08.003>
- [34] D. C. Look, *Electrical Characterization of GaAs Materials and Devices*, Wiley, New York, **1989**.
- [35] S. Lin, W. Li, Z. Chen, J. Shen, B. Ge, Y. Pei. *Nature Comm.* **2015**, *7*, 10287. <https://doi.org/10.1038/ncomms10287>
- [36] A. L. Efros, B. I. Shklovskii. *Electronic Properties of Doped Semiconductors*, Springer, Berlin, Germany, **1985**.
- [37] D. K. Sang, B. Wen, S. Gao, Y. Zeng, F. Meng, Z. Guo, H. Zhang. *Nanomaterials* **2019**, *9*, 1075. <https://doi.org/10.3390/nano9081075>
- [38] S. Tanuma. *Sci. Rep. Res. Inst. Tohoku Univ. Ser. A*, **1954**, *6*, 159–171.
- [39] B. P. Falcão, J. P. Leitão, M. R. Correia, M. R. Soares, F. M. Morales, J. M. Manuel, R. Garcia, A. Gustafsson, M. V. B. Moreira, A. G. de Oliveira, J. C. Gonzalez. *J. Appl. Phys.*, **2013**, *114*(18), 183508. <https://doi.org/10.1063/1.4829455>
- [40] A. C. S. Pimenta, D. C. Teles Ferreira, D. B. Roa, M. V. B. Moreira, A. G. de Oliveira, J. C. González, M. De Giorgi, D. Sanvitto, F. M. Matinaga. *J. Phys. Chem. C* **2016**, *120*, 30, 17046–17051. <https://doi.org/10.1021/acs.jpcc.6b04458>.
- [41] W. Hoerstel, D. Kusnick, M. Spitzer. High-Field Transport and Low-Field Mobility in Tellurium Single Crystals. *phys. stat. sol. (b)* **1973**, *60*, 213. <https://doi.org/10.1002/pssb.2220600123>
- [42] N. Zhang, G. Zhao, L. Li, P. Wang, L. Xie, B. Cheng, H. Li, Z. Lin, C. Xi, J. Ke, M. Yang, J. He, Z. Sun, Z. Wang, Z. Zhanga, C. Zenga. *PNAS* **2020**, *117*, 11337. <https://doi.org/10.1073/pnas.2002913117>
- [43] P. Skadron, V. A. Johnson. *J. Appl. Phys.* **1966**, *37*, 1912 (1966). <http://dx.doi.org/10.1063/1.1708624>
- [44] K. Takita, T. Hagiwara, S. Tanaka. *I. J. Phys. Soc. Jpn.* **1971**, *31*, 1469–1478. <https://doi.org/10.1143/JPSJ.34.1548>
- [45] P. Sun, C. Li, J. Xu, Q. Jiang, W. Wang, J. Liu, F. Zhao, Y. Ding, J. Houc, F. Jiang. *Sustainable Energy Fuels* **2018**, *2*, 2636. <https://doi.org/10.1039/c8se00297e>
- [46] A. Phahle. *Thin Solid Films* **1977**, *41*, 235–241. [https://doi.org/10.1016/0040-6090\(77\)90408-4](https://doi.org/10.1016/0040-6090(77)90408-4)
- [47] J. F. Oliveira, M. B. Fontes, M. Moutinho, S. E. Rowley, E. Baggio-Saitovitch, M. B. S. Neto, C. Enderlein. *Commun. Mater.* **2021**, *2*, 1. <https://doi.org/10.1038/s43246-020-00110-1>
- [48] E. R. Viana, J. C. González, G. M. Ribeiro, A. G. de Oliveira. *Phys. status solidi RRL* **2012**, *6*, 262–264. <https://doi.org/10.1002/pssr.201206161>
- [49] G. Zhou, R. Addou, Q. Wang, S. Honari, C. R. Cormier, L. Cheng, R. Yue, C. M. Smyth, A. Laturia, J. Kim, W. G. Vandenberghe, M. J. Kim, R. M. Wallace, and C. L. Hinkle, *Adv. Mater.* **2018**, *30*(36), 1803109. <https://doi.org/10.1002/adma.201803109>

- [50] F. Liang and H. Qian, *Mater. Chem. Phys.* **2009**, *113*(2), 523.  
<https://doi.org/10.1016/j.matchemphys.2008.07.101>
- [51] H. Tao, H. Liu, D. Qin, K. Chan, J. Chen, and Y. Cao, *J. Nanosci. Nanotechnol.* **2010**, *10*(12), 7997. <https://doi.org/10.1166/jnn.2010.3000>
- [52] K. R. Sapkota, P. Lu, D. L. Medlin, G. T. Wang. *APL Materials* **2019**, *7*, 081103  
<https://doi.org/10.1063/1.5109899>